

www.acsami.org Research Article

Exchange Bias in a La_{0.67}Sr_{0.33}MnO₃/NiO Heterointerface Integrated on a Flexible Mica Substrate

Jijie Huang,* Han Wang, Xuejing Wang, Xingyao Gao, Juncheng Liu, and Haiyan Wang*



Cite This: ACS Appl. Mater. Interfaces 2020, 12, 39920–39925



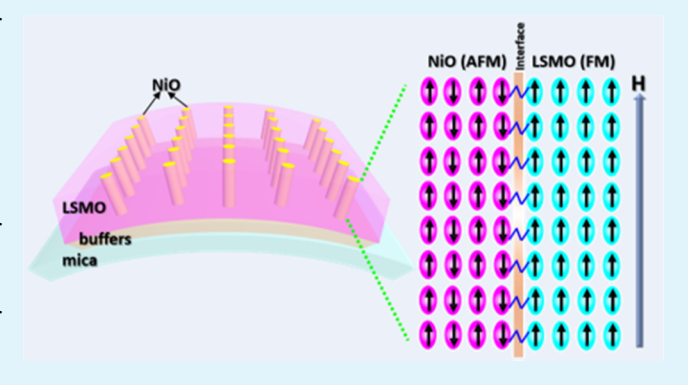
ACCESS

Metrics & More



Supporting Information

ABSTRACT: Flexible electronics integrating spintronics are of great potential in the areas of lightweight and flexible personal electronics. The integration of ferromagnetic and other functional oxides on flexible mica substrates is crucial for the proposed computer technology. In this work, we demonstrate the successful integration of a ferromagnetic—antiferromagnetic nanocomposite of La_{0.67}Sr_{0.33}MnO₃ (LSMO)/NiO with unique perpendicular exchange bias properties on a flexible mica substrate. Utilization of multiple sets of buffer layers has been attempted to overcome the large mismatch between the film and the substrate and to achieve high-quality nanocomposite growth on mica. Exchange bias of ~200 and ~140 Oe for the applied magnetic field perpendicular and parallel to the film surface, respectively, has been achieved and



attributed to the strongly coupled vertical ferromagnetic/antiferromagnetic interfaces. Such nanocomposite thin films exhibit excellent structural robustness and reliability under a cyclic bending test. This work demonstrates the enormous potential of integrating complex two-phase multifunctional oxides on mica for future flexible wearable personal devices.

KEYWORDS: flexible electronics, mica, exchange bias, nanocomposite thin film, pulsed laser deposition

■ INTRODUCTION

The design and fabrication of flexible, portable, and wearable devices are of great interest in the past few years. 1-3 Meanwhile, functional oxide thin film is one of the major material candidates for various electronic, spintronic, and photonic devices. However, high-quality oxide thin film always involves high-temperature growth process, which typically requires single crystalline oxide substrates with high thermal stability. 4-6 Such rigid single crystal oxide substrates are not ideal for the flexible device applications. To overcome this issue, two effective approaches have been demonstrated, that is, "thin film transferring" and "substrate treatment". For the former method, oxide thin films have been first deposited on a buffered substrate, then the buffer layer is dissolved or removed in certain solutions (e.g., water, etc.) to obtain a freestanding film, and finally, the freestanding film will be transferred on flexible substrates for further device integration and fabrication. 7-9 For the later method, oxide thin films were deposited on flexible metal foils, which have been fine-polished in advance. 10-12 However, it typically requires a set of buffer layers to overcome the large mismatch, inter-diffusion, and other issues. There is a great need to search for a flexible substrate with a high melting point for direct deposition of oxides.

Mica, a layered oxide material with a high melting point of $1300\,^{\circ}$ C, can be peeled off into thin layers with few atomic

layers, become flexible, and thus can be considered as an effective solution. Various oxide thin films have been successfully deposited on mica with excellent film quality and interesting physical properties, including Sn-doped In₂O₃ (ITO),¹³ La_{0.67}Sr_{0.33}MnO₃ (LSMO),¹⁴ SrRuO₃ (SRO),¹⁵ CoFe₂O₄ (CFO),¹⁶ Pb(Zr,Ti)O₃ (PZT),¹⁷ and so forth. However, multifunctional nanocomposite thin films on mica are rarely deposited or reported; up to date, only Amrillah *et al.* has grown BiFeO₃–CoFe₂O₄ nanocomposite on mica ¹⁸ because of the challenges of the cogrowth of two oxides. Thus, integrating nanocomposite thin film on mica is of great importance for coupling multifunctionalities on flexible mica substrates. ^{19–21}

In this work, we have deposited a nanocomposite of $(LSMO)_{0.5}/(NiO)_{0.5}$ (L5N5) on flexible mica substrates with or without buffer layers. The basic concept is shown in Figure 1. The left and middle panels present an actual photograph and a schematic illustration of the sample on a bended mica, respectively, while the right schematic illustration demonstrates

Received: July 17, 2020 Accepted: August 6, 2020 Published: August 6, 2020





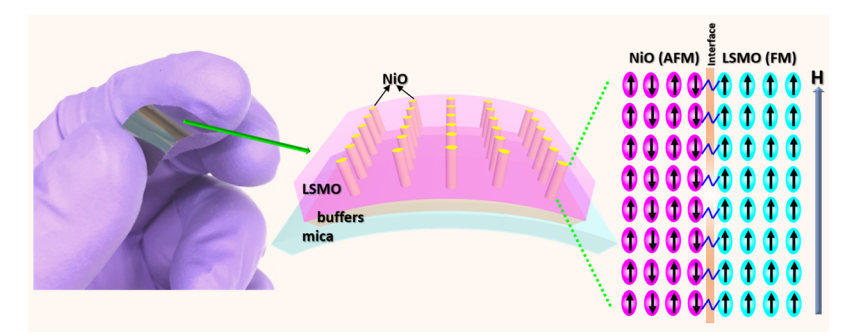


Figure 1. Conceptual demonstration of this study. The left panel presents a photograph of an actual sample in a bending condition, the middle panel exhibits a schematic illustration of the sample in a bending condition, and the right panel shows the exchange bias effect in the interface of LSMO and NiO with applied field (*H*) perpendicular to the film surface.

the exchange bias (EB) effect of the deposited L5N5 nanocomposite. As known, LSMO is ferromagnetic (FM)²² and NiO is antiferromagnetic (AFM), 23 and therefore, EB effect takes place by the spin interaction between the FM LSMO phase and AFM NiO phase, which has been demonstrated on SrTiO₃ (STO)²⁴ and Si substrates.²⁵ It is believed that a glass-like state (resulting from the competition between magnetic orders and spin frustration in the heterointerface) could pin the FM ordering and result in EB effect, which has been realized in the previous reported SrMnO₃/LSMO bilayer²⁶ and LSMO/La₂CuO₄ superlattice.²⁷ EB effect has extensive potential in various device applications, such as magnetic recording head for hard disk drive, magnetic field sensor, and magnetic random access memory. 28-30 The demonstration of such LSMO/NiO nanocomposite thin film on flexible mica is quite different from the prior reported nanocomposite systems on rigid single crystalline substrates. 24,25,31,32 The deposition on mica requires special care and a buffer layer stack to enable the high-quality growth. Robust perpendicular exchange bias has been achieved, which is different from the reported lateral exchange bias of Fe₃O₄/ BiFeO₃ multilayer on mica.³³ This work paves a way toward future flexible EB-based devices and lays a foundation for the fabrication of other complex nanocomposite thin film on flexible mica substrates.

■ RESULTS AND DISCUSSION

We first deposited L5N5 thin film directly on mica as a reference sample. The green curve in Figure 2 presents its θ - 2θ XRD result. Only mica (0 0 l) peaks and no obvious film peaks can be observed, except a minor peak at around 40.5° from LSMO (1 1 1), which suggests low crystallinity in the film. To achieve better film quality, a set of buffer layers have been explored, such as STO, STO/CFO and SRO/CFO. The XRD results in Figure 2 show LSMO (1 1 1) and NiO (1 1 1) peaks, despite the fact that LSMO (0 1 1) and LSMO (0 0 1) have been observed in L5N5 on STO buffer mica, which indicates the polycrystalline LSMO phase in the sample. However, in L5N5/SRO/CFO/mica and L5N5/STO/CFO/ mica samples, the LSMO phase could be considered as textured because only the LSMO (1 1 1) peak is obtained. It is also noted that there is a set of small periodical peaks in between the major periodical peaks from mica (0 0 l), which could be attributed to mica (0 0 2.5), (0 0 3.5), and so on. These small periodical peaks have only been observed in some of the mica substrates, which is because the quality of the original mica substrates varies slightly from piece to piece.

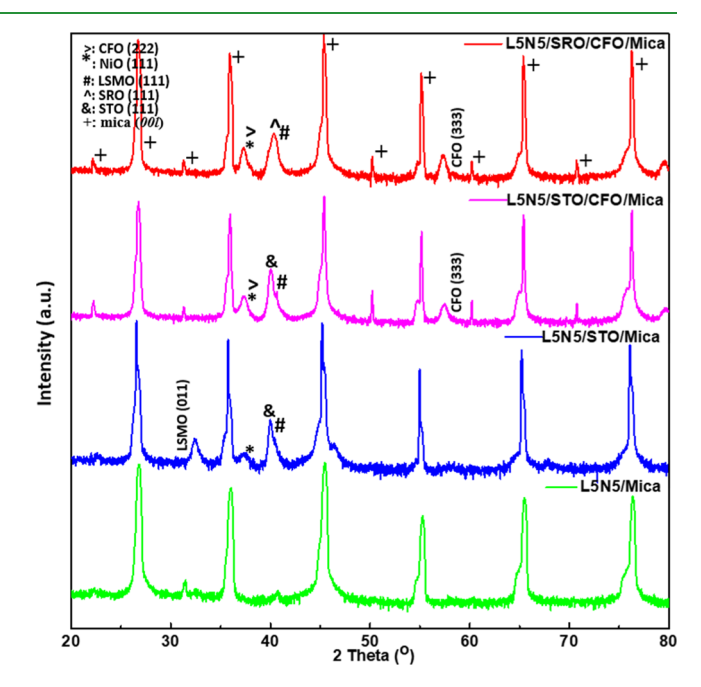


Figure 2. Standard θ –2 θ XRD scans of L5N5 thin films on various buffered mica substrates.

These results indicate that the buffer layers could effectively improve the film quality of L5N5; in addition, SRO can also serve as the bottom electrode for further device integration.

TEM characterization has been carried out to explore the microstructure of the L5N5 films on mica with different buffers. Figure 3a presents a low-magnification cross-sectional TEM image of L5N5 on SRO/CFO buffered mica; the thickness of each layer can be estimated to be \sim 15, \sim 35, and ~180 nm for CFO, SRO, and L5N5, respectively. The L5N5 film exhibits a vertically aligned nanocomposite (VAN) structure, which is, very fine NiO nanopillars appear in the LSMO matrix, as marked by the white arrows in Figure 3b. Figure 3b enlarges the interface region of the layers; clean and abrupt interfaces have been observed between each layer, which suggests that no or very limited interdiffusion occurs between different layers, and each layer exhibits excellent crystal quality. Coupled with the TEM and XRD data above, the LSMO/NiO nanocomposite has grown in the VAN form on mica. Figure 3c presents a low-magnification TEM image of L5N5 thin film on STO buffered mica, which also shows a VAN structure with a clean interface (note that in such TEM samples, the mica layer and most of the STO layer have been

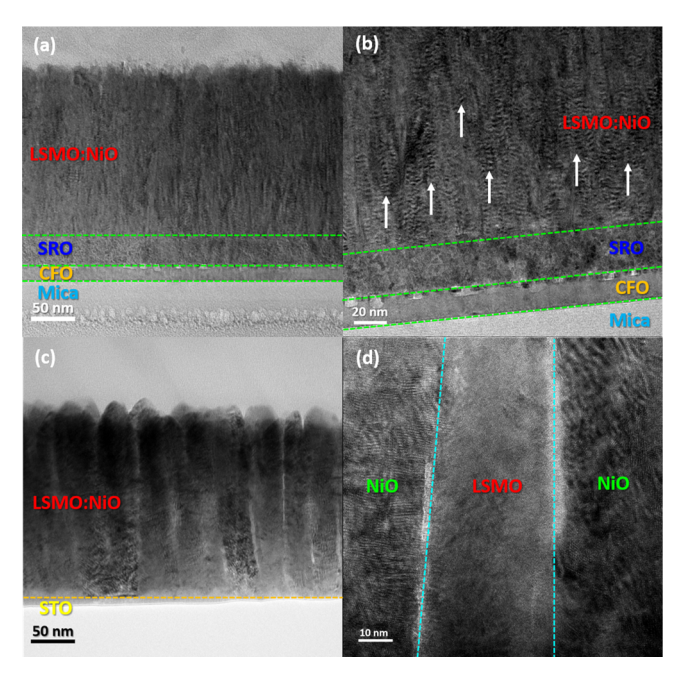


Figure 3. Microstructure characterization on the L5N5 thin film on buffered mica substrates. (a) Low-magnification and (b) medium-magnification TEM images taken near the interface region of L5N5 on SRO/CFO buffered mica; (c) low-magnification and (d) high-resolution TEM images of L5N5 on the STO buffered mica substrate.

damaged by ion milling process). A high-magnification TEM image in Figure 3d exhibits a typical local area; the two phases of LSMO and NiO are grown separately and alternatively; the phases of LSMO and NiO can be identified by the contrast of the image (the contrast is typically inverse to the atomic number Z of the material in the TEM mode). The microstructure of the L5N5 film grown on STO/CFO buffered mica is also shown in Figure S1, VAN-like structure is also observed, and the thickness of each layer can be estimated to be \sim 30, \sim 35, and \sim 220 nm for CFO, SRO, and L5N5, respectively. Furthermore, the surface morphology of all the samples have been explored by atomic force microscopy (AFM) characterization, as shown in Figures S2-S5 for L5N5/SRO/CFO/mica, L5N5/STO/CFO/mica, L5N5/ STO/mica, and L5N5/mica, respectively. The surface morphology of the samples mostly remain the same after 100 times of bending. It is also noted that the measured samples are small pieces cut from the large virgin pieces, which might also cause minor difference from different areas.

Then, EB effect of the L5N5 nanocomposite thin films deposited on different buffered mica has been investigated by measuring the magnetization-field (M-H) hysteresis loops, the measurements were taken after a field cooling of 1 T down to 10 K. Magnetic field (-8000-8000 Oe) has been applied in either OP (perpendicular to film surface) or IP (parallel to film surface) direction, and the results are plotted in Figure 4a,b, respectively. Based on the M-H curves, the H_{EB} value can be calculated by $H_{\rm EB} = |H_+ + H_-|/2$ (here, H_+ and H_- represent the positive and negative values of coercivity, where the magnetization becomes zero). All the films exhibit EB effect, with the one on STO/CFO buffered mica obtaining the highest OP $H_{\rm EB}$ value of ~210 Oe and IP $H_{\rm EB}$ value of ~140 Oe (as shown in the inset of Figure 4a,b), which is in the same range of LSMO/NiO nanocomposite films on single crystalline STO or Si substrates. 24,25,31,32 The reason is that such sample obtains the best crystallinity with the STO/CFO buffer layers, and the lattice mismatch induced tensile strain for LSMO domains could also stabilize the FM ordering and hence lead to higher EB values.³⁴ The TEM images of the buffers in Figure S6 further confirms that the crystallinity of the STO/ CFO buffer layer stack (Figure S6a) is better than SRO/CFO (Figure S6b). The relatively low crystallinity of the SRO layer could be due to the potential interdiffusion between the CFO and SRO layers and the ion milling damage during the final ion-polishing step during TEM sample preparation. The STO/ CFO shows excellent crystallinity. Furthermore, the surface uncompensated magnetic moment of the AFM NiO nanopillars could also contribute to the overall EB properties.³⁵ On the other hand, for all the measured films, the OP $H_{\rm EB}$ value is higher than IP H_{EB} value owing to the OP anisotropic nature of the L5N5 film, and the EB effect is dominant at the vertical interface, which has the same trend compared to the LSMO-NiO nanocomposite films grown on rigid STO and Si substrates. 25,3

The major advantage of flexible devices over rigid devices (such as Si based device) is their flexibility, which means it can undergo bending upon usage. Therefore, it is critical to explore the robustness and stability of L5N5 film under bending conditions, that is, concave or convex bending. Taking the sample of L5N5 on STO/CFO buffered mica as an example, we first peeled off the mica substrate into few layers to make it bendable, and then the flexible samples were attached on curved plastic models (radius of ~14 mm). Either convex or concave condition has been applied, as illustrated in the inset of Figure 5a,b, respectively. M-H measurement was conducted and compared for the virgin sample and the same sample

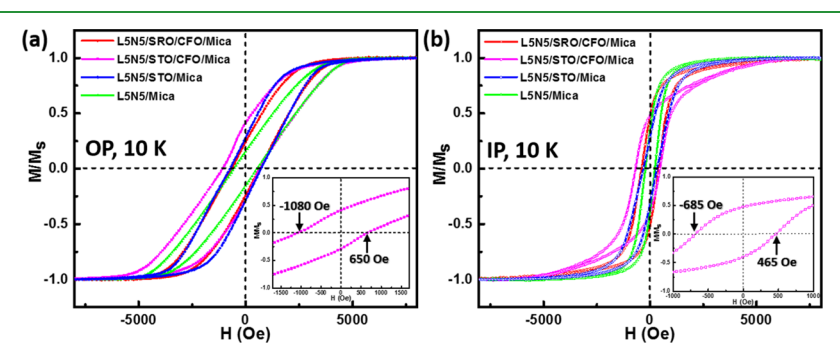


Figure 4. Normalized magnetic hysteresis loops of L5N5 thin films grown on different buffered mica substrates measured at 10 K with applied magnetic field in (a) OP and (b) IP directions. The inset shows the central enlarged area of the L5N5 on STO/CFO buffered mica sample to show the exchange bias value.

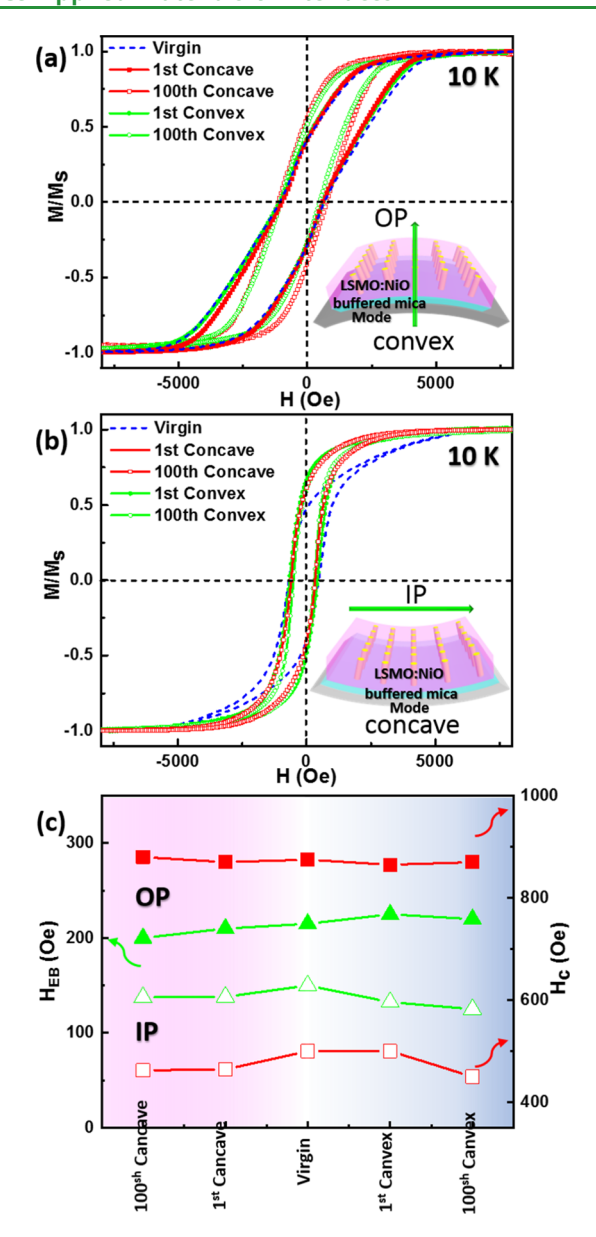


Figure 5. Normalized magnetic hysteresis loops at 10 K with applied field in (a) OP and (b) IP directions of the virgin sample and with bending (concave or convex) once and 100 times for L5N5 on STO/CFO buffered mica; (c) comparison of exchange bias value and coercivity value of the sample with (once or 100 times) and without bending conditions.

under bending conditions. To investigate the long-term stability and reliability, the sample was further bent 100 times before taking another measurement. All M-H curves are plotted in Figure 5a for applying OP magnetic field and Figure 5b for applying IP magnetic field. As seen, there is no significant change in the M-H curves even after bending 100 times for both OP and IP, which reveals the robustness of the L5N5 nanocomposite on mica. However, the shape of M-H curves under OP and IP magnetic field is very different, which is related to the nanostructure of VANs. The results of all the samples with or without bending are compared in Figure 5c (left axis, green solid triangle for OP and green hollow triangle for IP). The $H_{\rm EB}$ value of the sample after bending (1 time or 100 times) remains similar to that of the virgin sample, ~210 Oe for OP and ~140 Oe for IP, which again demonstrates the

stability and reliability of the mica integration. Lastly, coercivity $(H_{\rm C})$ values of virgin L5N5 and under bending conditions were calculated by $H_{\rm C}=|H_+-H_-|/2$ and are compared in Figure 5c (red solid square for OP and red hollow square for IP). The OP $H_{\rm C}$ also obtains a much higher value of ~865 Oe than the IP $H_{\rm C}$ of ~575 Oe, which is also due to the out-of-plane preferred anisotropy of the L5N5 film. Overall, the L5N5 nanocomposite film on flexible mica exhibits obvious EB effect resulting from the spin interaction at the FM-AFM interface, and such EB effect is very robust and reliable under bending conditions, which indicates its promising potential for future flexible device integration.

The quality of L5N5 nanocomposite thin film directly grown on mica is not as good as the one deposited on the singlecrystal STO substrate, from the crystallinity point of view. 24,31 After introducing the buffer layers, the film quality greatly improves and its $H_{\rm EB}$ value is even higher than the previous reported 77 Oe for the L5N5 on single-crystal STO.31 Furthermore, selected conductive oxides could serve as buffer layers for the nanocomposite thin film growth; meanwhile, it can also work as the bottom electrode for flexible device integration. The successful demonstration of L5N5 with exchange bias effect on flexible mica is quite promising as only the BiFeO₃/CoFe₂O₄ nanocomposite has been previously deposited on mica for multiferroics. 18 This study provides the strategy to design other multifunctional nanocomposite thin films for future flexible electronic integration and for appropriate buffer selection for achieving desired performance.

CONCLUSIONS

LSMO/NiO nanocomposite thin films have been successfully deposited on flexible mica substrates for potential flexible device applications. Different buffer layers have been explored and compared to satisfy the lattice matching and thus obtain high-quality thin films. Exchange bias (EB) effect has been induced because of the spin interaction at the vertical heterointerface of the FM LSMO phase and the AFM NiO phase. The EB value in the perpendicular direction (~200 Oe) is higher than that of the parallel direction (~140 Oe), owing to the nanopillar-in-matrix structure of the film. Furthermore, no obvious reduction in the EB value has been observed after different bending conditions, which reveals excellent robustness and reliability of the nanocomposite thin film. The complex nanocomposite thin films integrated on mica could be further developed for other systems beyond exchange biasbased flexible devices.

EXPERIMENTAL SECTION

The (LSMO)_{0.5}(NiO)_{0.5} nanocomposite target was made by conventional solid-state mixing; LSMO and NiO powders were mixed at a molar ratio of 50:50. Then, the mixed powders were pressed into a pellet (1 in. diameter) and sintered at 1200 °C for 6 h. The LSMO-NiO nanocomposite thin films were deposited on mica (2 cm × 2 cm) with or without buffers using the pulsed laser deposition technique with a KrF excimer laser (Lambda Physik, $\lambda = 248$ nm). Before deposition, the base pressure was below 1×10^{-6} Torr. The deposition parameters are as follows: deposition temperature was 700 °C, the target-substrate distance was 4.5 cm, the deposition frequency was 5 Hz, oxygen pressure was 100 mTorr, and the sample was cooled in 200 Torr oxygen at 10 °C/min after the deposition. The deposition condition for the CFO, SRO, and STO buffers is listed below: deposition temperature of 700 °C, the target-substrate distance was 4.5 cm, the deposition frequency was 10 Hz, and oxygen pressure was 20 mTorr for CFO and 100 mTorr for SRO and STO. The crystal structure and microstructure of the films were studied by XRD (Panalytical X'Pert X-ray diffractometer) and TEM (FEI Talos-200X). The magnetic hysteresis loops were measured by a SQUID magnetometer (MPMS: Quantum Design) using cut samples (5 mm × 5 mm).

ASSOCIATED CONTENT

Supporting Information

The Supporting Information is available free of charge at https://pubs.acs.org/doi/10.1021/acsami.0c12935.

STEM images of the LSN5/STO/CFO sample; AFM images of L5N5/SRO/CFO/mica, L5N5/STO/CFO/mica, L5N5/STO/mica, and L5N5/mica thin films; and TEM images of L5N5/STO/CFO/mica and L5N5/SRO/CFO/mica samples (PDF)

AUTHOR INFORMATION

Corresponding Authors

Jijie Huang — School of Materials, Sun Yat-Sen University, Guangzhou, Guangdong 510275, China; School of Materials Engineering, Purdue University, West Lafayette, Indiana 47907, United States; Email: huangjj83@mail.sysu.edu.cn

Haiyan Wang — School of Materials Engineering and School of Electrical and Computer Engineering, Purdue University, West Lafayette, Indiana 47907, United States; orcid.org/0000-0002-7397-1209; Email: hwang00@purdue.edu

Authors

Han Wang — School of Materials Engineering, Purdue University, West Lafayette, Indiana 47907, United States; orcid.org/0000-0002-6137-4802

Xuejing Wang — School of Materials Engineering, Purdue University, West Lafayette, Indiana 47907, United States

Xingyao Gao – School of Materials Engineering, Purdue University, West Lafayette, Indiana 47907, United States

Juncheng Liu – School of Materials Engineering, Purdue University, West Lafayette, Indiana 47907, United States

Complete contact information is available at: https://pubs.acs.org/10.1021/acsami.0c12935

Notes

The authors declare no competing financial interest.

■ ACKNOWLEDGMENTS

The work was supported by the U.S. National Science Foundation (Ceramic Program, DMR-1565822 and DMR-2016453). J.H. acknowledges the support from Guangdong Basic and Applied Basic Research Foundation (2019A1515111029) and the startup funding at Sun Yat-Sen University (76180-18841219).

■ REFERENCES

- (1) Son, D.; Lee, J.; Qiao, S.; Ghaffari, R.; Kim, J.; Lee, J. E.; Song, C.; Kim, S. J.; Lee, D. J.; Jun, S. W.; Yang, S.; Park, M.; Shin, J.; Do, K.; Lee, M.; Kang, K.; Hwang, C. S.; Lu, N.; Hyeon, T.; Kim, D.-H. Multifunctional Wearable Devices for Diagnosis and Therapy of Movement Disorders. *Nat. Nanotechnol.* **2014**, *9*, 397–404.
- (2) Gao, W.; Emaminejad, S.; Nyein, H. Y. Y.; Challa, S.; Chen, K.; Peck, A.; Fahad, H. M.; Ota, H.; Shiraki, H.; Kiriya, D.; Lien, D.-H.; Brooks, G. A.; Davis, R. W.; Javey, A. Fully Integrated Wearable Sensor Arrays for Multiplexed in situ Perspiration Analysis. *Nature* **2016**, *529*, 509–514.

- (3) Fan, F. R.; Tang, W.; Wang, Z. L. Flexible Nanogenerators for Energy Harvesting and Self-powered Electronics. *Adv. Mater.* **2016**, 28, 4283–4305.
- (4) Martin, L. W.; Chu, Y.-H.; Ramesh, R. Advances in the Growth and Characterization of Magnetic, Ferroelectric, and Multiferroic Oxide Thin Films. *Mater. Sci. Eng., R* **2010**, *68*, 89–133.
- (5) Huang, J.; Wang, H. Effective magnetic pinning schemes for enhanced superconducting property in high temperature superconductor YBa2Cu3O7-x: a review. *Supercond. Sci. Technol.* **2017**, 30, 114004.
- (6) Choi, K. J.; Biegalski, M.; Li, Y. L.; Sharan, A.; Schubert, J.; Uecker, R.; Reiche, P.; Chen, Y. B.; Pan, X. Q.; Gopalan, V.; Chen, L. Q.; Schlom, D. G.; Eom, C. B. Enhancement of Ferroelectricity in Strained BaTiO3 Thin Films. *Science* **2004**, *306*, 1005–1009.
- (7) Shen, L.; Wu, L.; Sheng, Q.; Ma, C.; Zhang, Y.; Lu, L.; Ma, J.; Ma, J.; Bian, J.; Yang, Y.; Chen, A.; Lu, X.; Liu, M.; Wang, H.; Jia, C.-L. Epitaxial Lift-off of Centimeter-scaled Spinel Ferrite Oxide Thin Films for Flexible Electronics. *Adv. Mater.* **2017**, *29*, 1702411.
- (8) Lee, D. K.; Kim, S.; Oh, S.; Choi, J.; Lee, J.; Yu, H. Water-soluble Epitaxial NaCl Thin Film for Fabrication of Flexible Devices. *Sci. Rep.* **2017**, *7*, 8716.
- (9) Lu, D.; Baek, D. J.; Hong, S. S.; Kourkoutis, L. F.; Hikita, Y.; Hwang, H. Y. Synthesis of Freestanding Single-crystal Perovskite Films and Heterostructures by Etching of Sacrificial Water-soluble Layers. *Nat. Mater.* **2016**, *15*, 1255–1260.
- (10) Wee, S. H.; Huang, P.-S.; Lee, J.-K.; Goyal, A. Heteroepitaxial Cu₂O Thin Film Solar Cell on Metallic Substrates. *Sci. Rep.* **2015**, *5*, 16272.
- (11) Huang, J.; Chen, L.; Jian, J.; Khatkhatay, F.; Jacob, C.; Wang, H. A Simplified Superconducting Coated Conductor Design with Febased Superconductors on Glass and Flexible Metallic Substrates. *J. Alloys Compd.* **2015**, *647*, 380–385.
- (12) Dutta, P.; Rathi, M.; Zheng, N.; Gao, Y.; Yao, Y.; Martinez, J.; Ahrenkiel, P.; Selvamanickam, V. High Mobility Single-crystalline-like GaAs Thin Films on Inexpensive Flexible Metal Substrates by Metalorganic Chemical Vapor Deposition. *Appl. Phys. Lett.* **2014**, *105*, 092104.
- (13) Ke, S.; Chen, C.; Fu, N.; Zhou, H.; Ye, M.; Lin, P.; Yuan, W.; Zeng, X.; Chen, L.; Huang, H. Transparent Indium Tin Oxide Electrodes on Muscovite Mica for High-temperature-processed Flexible Optoelectronic Devices. ACS Appl. Mater. Interfaces 2016, 8, 28406–28411.
- (14) Huang, J.; Wang, H.; Sun, X.; Zhang, X.; Wang, H. Multifunctional La0.67Sr0.33MnO3 (LSMO) Thin Films Integrated on Mica Substrates toward Flexible Spintronics and Electronics. ACS Appl. Mater. Interfaces 2018, 10, 42698–42705.
- (15) Liu, J.; Feng, Y.; Tang, R.; Zhao, R.; Gao, J.; Shi, D.; Yang, H. Mechanically Tunable Magnetic Properties of Flexible SrRuO3 Epitaxial Thin Films on Mica Substrates. *Adv. Electron. Mater.* **2018**, *4*, 1700522.
- (16) Liu, H.-J.; Wang, C.-K.; Su, D.; Amrillah, T.; Hsieh, Y.-H.; Wu, K.-H.; Chen, Y.-C.; Juang, J.-Y.; Eng, L. M.; Jen, S.-U.; Chu, Y.-H. Flexible Heteroepitaxy of CoFe2O4/Muscovite Bimorph with Large Magnetostriction. ACS Appl. Mater. Interfaces 2017, 9, 7297–7304.
- (17) Jiang, J.; Bitla, Y.; Huang, C.-W.; Do, T. H.; Liu, H.-J.; Hsieh, Y.-H.; Ma, C.-H.; Jang, C.-Y.; Lai, Y.-H.; Chiu, P.-W.; Wu, W.-W.; Chen, Y.-C.; Zhou, Y.-C.; Chu, Y.-H. Flexible Ferroelectric Element Based on van der Waals Heteroepitaxy. *Sci. Adv.* **2017**, 3, No. e1700121.
- (18) Amrillah, T.; Bitla, Y.; Shin, K.; Yang, T.; Hsieh, Y.-H.; Chiou, Y.-Y.; Liu, H.-J.; Do, T. H.; Su, D.; Chen, Y.-C.; Jen, S.-U.; Chen, L.-Q.; Kim, K. H.; Juang, J.-Y.; Chu, Y.-H. Flexible Multiferroic Bulk Heterojunction with Giant Magnetoelectric Coupling via van der Waals Epitaxy. ACS Nano 2017, 11, 6122–6130.
- (19) Huang, J.; MacManus-Driscoll, J. L.; Wang, H. New Epitaxy Paradigm in Epitaxial Self-assembled Oxide Vertically Aligned Nanocomposite Thin Films. *J. Mater. Res.* **2017**, *32*, 4054–4066.
- (20) MacManus-Driscoll, J. L. Self-assembled Heteroepitaxial Oxide Nanocomposite Thin Film Structures: Designing Interface-induced

- Functionality in Electronic Materials. Adv. Funct. Mater. 2010, 20, 2035–2045.
- (21) Chen, A.; Bi, Z.; Jia, Q.; MacManus-Driscoll, J. L.; Wang, H. Microstructure, Vertical Strain Control and Tunable Functionalities in Self-assembled, Vertically Aligned Nanocomposite Thin Films. *Acta Mater.* **2013**, *61*, 2783.
- (22) Thiele, C.; Dorr, K.; Bilani, O.; Rodel, J.; Schultz, L. Influence of Strain on the Magnetization and Magnetoelectric Effect in La_{0.7}A_{0.3}MnO₃/PMN-PT(001) (A=Sr, Ca). *Phys. Rev. B: Condens. Matter Mater. Phys.* **2007**, 75, 054408.
- (23) Satoh, T.; Cho, S. J.; Iida, R.; Shimura, T.; Kuroda, K.; Ueda, H.; Ueda, Y.; Ivanov, B. A.; Nori, F.; Fiebig, M. Spin Oscillations in Antiferromagnetic NiO Triggered by Circularly Polarized Light. *Phys. Rev. Lett.* **2010**, *105*, 077402.
- (24) Ning, X.; Wang, Z.; Zhang, Z. Large, Temperature-Tunable Low-Field Magnetoresistance in La0.7Sr0.3MnO3:NiO Nanocomposite Films Modulated by Microstructures. *Adv. Funct. Mater.* **2014**, *24*, 5393–5401.
- (25) Huang, J.; Gellatly, A.; Kauffmann, A.; Sun, X.; Wang, H. Exchange Bias Effect along Vertical Interfaces in La0.7Sr0.3MnO3:-NiO Vertically Aligned Nanocomposite Thin Films Integrated on Silicon Substrates. *Cryst. Growth Des.* **2018**, *18*, 4388–4394.
- (26) Ding, J. F.; Lebedev, O. I.; Turner, S.; Tian, Y. F.; Hu, W. J.; Seo, J. W.; Panagopoulos, C.; Prellier, W.; Van Tendeloo, G.; Wu, T. Interfacial Spin Glass State and Exchange Bias in Manganite Bilayers with Competing Magnetic Orders. *Phys. Rev. B: Condens. Matter Mater. Phys.* **2013**, 87, 054428.
- (27) Ding, J.; Cossu, F.; Lebedev, O. I.; Zhang, Y.; Zhang, Z.; Schwingenschlögl, U.; Wu, T. Manganite/Cuprate Superlattice as Artificial Reentrant Spin Glass. *Adv. Mater. Interfaces* **2016**, 3, 1500676.
- (28) Chappert, C.; Fert, A.; Van Dau, F. N. The Emergence of Spin Electronics in Data Storage. *Nat. Mater.* **2007**, *6*, 813–823.
- (29) Dery, H.; Dalal, P.; Cywiński, Ł.; Sham, L. J. Spin-based Logic in Semiconductors for Reconfigurable Large-scale Circuits. *Nature* **2007**, 447, 573–576.
- (30) Röbisch, V.; Yarar, E.; Urs, N. O.; Teliban, I.; Knöchel, R.; McCord, J.; Quandt, E.; Meyners, D. Exchange Biased Magnetoelectric Composites for Magnetic Field Sensor Application by Frequency Conversion. *J. Appl. Phys.* **2015**, *117*, 17B513.
- (31) Zhang, W.; Li, L.; Lu, P.; Fan, M.; Su, Q.; Khatkhatay, F.; Chen, A.; Jia, Q.; Zhang, X.; MacManus-Driscoll, J. L.; Wang, H. Perpendicular Exchange-Biased Magnetotransport at the Vertical Heterointerfaces in La0.7Sr0.3MnO3:NiO Nanocomposites. ACS Appl. Mater. Interfaces 2015, 7, 21646–21651.
- (32) Ning, X. K.; Wang, Z. J.; Zhao, X. G.; Shih, C. W.; Zhang, Z. D. Exchange bias in La0.7Sr0.3MnO3/NiO and LaMnO3/NiO interfaces. *J. Appl. Phys.* **2013**, *113*, 223903.
- (33) Zheng, W. C.; Zheng, D. X.; Wang, Y. C.; Li, D.; Jin, C.; Bai, H. L. Flexible Fe3O4/BiFeO3 multiferroic heterostructures with uniaxial strain control of exchange bias. *J. Magn. Magn. Mater.* **2019**, *481*, 227–233
- (34) Fang, Z.; Solovyev, I. V.; Terakura, K. Phase Diagram of Tetragonal Manganites. *Phys. Rev. Lett.* **2000**, *84*, 3169.
- (35) Huang, X. H.; Ding, J. F.; Zhang, G. Q.; Hou, Y.; Yao, Y. P.; Li, X. G. Size-dependent Exchange Bias in La_{0.25}Ca_{0.75}MnO₃ Nanoparticles. *Phys. Rev. B: Condens. Matter Mater. Phys.* **2008**, *78*, 224408.